Pergamon

PII: S1359-6454(96)00281-9

Acta mater. Vol. 45, No. 4. pp. 1535–1549, 1997

Published by Elsevier Science Ltd

1359-6454/97 $17.00 + 0.00

ON THE SOLIDIFICATION OF DENDRITIC ARRAYS: AN ASYMPTOTIC THEORY FOR THE DIRECTIONAL SOLIDIFICATION OF SLENDER NEEDLE CRYSTALS

BRIAN J. SPENCER† and HERBERT E. HUPPERT

Institute of Theoretical Geophysics, Department of Applied Mathematics and Theoretical Physics, University of Cambridge, Silver Street, Cambridge CB3 9EW, U.K.

(Received 3 January 1996; accepted form 3 July 1996)

Abstract—We consider a mathematical model for directional solidification of a binary alloy as a periodic array of three-dimensional needle crystals. Arguing from an analysis of published experimental data for dendritic growth, we identify a natural separation of characteristic length scales for dendrites. We use these observed disparities in length scales to define a small parameter for dendritic growth and identify scalings for all the process parameters in terms of this small parameter. We then solve the resulting free boundary problem using matched asymptotic expansions. Our analysis results in an integral equation for the shape of the needle crystal. We suggest that the integral equation contains a mechanism for the unique selection of the tip radius of the needle crystal independent of surface energy. This is in sharp contrast to previous studies regarding determination of the tip radius of an isolated, single-component, isothermal dendrite. Our results suggest that selection of the tip radius is linked to the spacing of the array. © *1997 Acta Metallurgica Inc.*

1. INTRODUCTION

This paper is concerned with the prediction of dendritic morphologies during the directional solidification of a binary alloy. Our approach is to find smooth, steady-state needle crystal shapes which form an underlying basis for the more complicated dendrite morphology. The presence of sidebranches on the dendrite is presumed to be the result of a sidebranching instability which develops on the smooth needle crystal. The description of needle crystal morphologies thus has two purposes. The first purpose is for use as a "basic state" in the description of the sidebranching instability. The second purpose, which is of central concern to us here, is for use in predicting the morphology characteristics of dendritic growth such as the tip radius, array spacing, tip undercooling and overall dendrite shape. Just as the Ivantsov isolated needle crystal solution [1] is sometimes referred to as a "dendrite", we shall also refer to the smooth needle crystal shapes in our array as "dendrites". For a further discussion of the philosophy behind using needle crystals to model dendritic growth, see Ref. [2].

We shall obtain smooth, needle crystal shapes as a solution to a mathematical model describing directional solidification. The mathematical model is a free boundary problem, and is not very easily solved in general. In particular there are three experimental length scales and four morphological length scales that conspire to make the full problem very difficult. Our approach will be to examine the typical values of these length scales from published experimental results. By noticing a natural separation in length scales, we are able to identify a characteristic small parameter for dendritic growth and determine consistent scalings for all the parameters. We are then able to solve the problem using matched asymptotic expansions. The result of our analysis is an integral equation for the shape of the dendrite. This equation and its solutions have a particularly important implication for dendritic growth: the tip radius of the dendrite appears to be selected by the array spacing and *not* by the surface energy. This is possibly the most important conclusion of our study.

The paper is organized as follows. In Section 2 we describe the mathematical model of solidification. In Section 3 we analyse the different length scales in the problem, determine appropriate scalings for the parameters and formulate a set of scaled equations. In Section 4 we solve the equations using matched asymptotic expansions to derive an integral equation for the shape of the dendrite. Finally, in Section 5 we summarize our results and discuss the ramifications of the integral equation and its solutions to the selection of the dendrite tip characteristics. In a further paper we determine the numerical solutions of the integral equation and compare our predictions to experimental data [3].

†Present address: Department of Mathematics; SUNY at Buffalo; Buffalo, NY 14214-3094, U.S.A.

2. THE MODEL

We consider the directional solidification of a binary alloy with a morphology consisting of an array of needle crystals. The coordinate system travels with the solidification front in the $-z$ direction at constant speed V (see Fig. 1). In the moving frame there is an imposed temperature gradient with warmer liquid ahead of the front. The control variables are the alloy composition C_∞, the growth speed V, and the temperature gradient G.

The governing equations for the system are derived from the one-sided, frozen temperature model for directional solidification [4]. In this model, there is no diffusion of solute in the solid, and the imposed temperature field T is linear in z. The linear temperature profile corresponds to equal thermal diffusivities in the solid and liquid phases with the diffusion of heat being much more rapid than the diffusion of solute. The model further assumes that there is no fluid flow, no density change upon solidification, and that the phase diagram is composed of straight lines (see Fig. 2). The concentration of solute $C(x, y, z, t)$ satisfies the following equations in the moving coordinate frame. First, the concentration satisfies the advection–diffusion equation,

$$\frac{\partial C}{\partial t} = D\nabla^2 C - V\frac{\partial C}{\partial z} \quad \text{in } \mathscr{L} \tag{1}$$

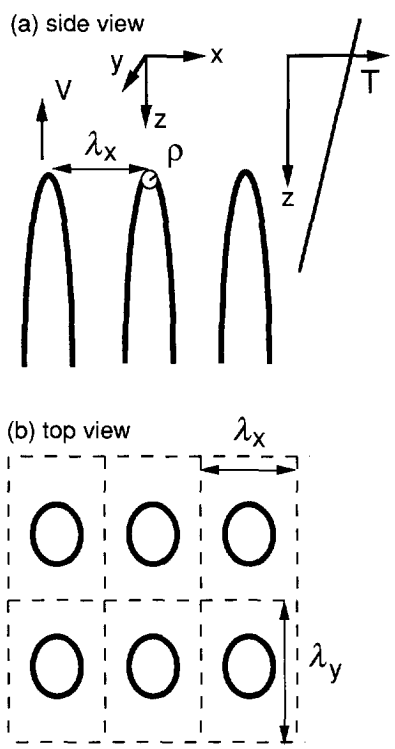

Fig. 1. Schematic of an array of needle crystals. (a) Side view, (b) top view.

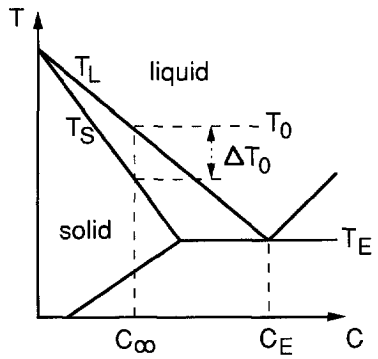

Fig. 2. Phase diagram used in the model.

where D is the solute diffusivity in the liquid and $\mathscr{L}$ denotes the liquid region. One boundary condition on the system is that the solid–liquid interface $\mathscr{B}$ is in local equilibrium, as given by the Gibbs–Thomson condition,

$$T = T_M + m_L C - \Gamma\kappa \quad \text{on } \mathscr{B} \tag{2}$$

where T is the temperature, T_M is the melting temperature of the pure material, m_L is the liquidus slope from the phase diagram, Γ is a surface energy/capillary constant which has units of temperature/length, and κ is the interfacial curvature. A second boundary condition is conservation of solute at the solidifying interface, with solute rejection balanced by the diffusion of solute away from the interface, as given by

$$(V_n - Vn_z)C(1-k) = -D(\mathbf{n}\cdot\nabla C) \quad \text{on } \mathscr{B} \tag{3}$$

where $\mathbf{n}$ is the unit normal vector of $\mathscr{B}$ pointing into the liquid, n_z is the component of $\mathbf{n}$ in the $+z$ direction, V_n is the normal velocity of the surface in the moving frame, and $k = (dT_L/dC)/(dT_S/dC)$ is the segregation coefficient from the phase diagram. Far ahead of the solidification front we require that the solute field decays to the mean alloy composition C_∞:

$$C \to C_\infty \quad \text{as} \quad z \to -\infty. \tag{4}$$

Finally, the frozen-temperature approximation prescribes the temperature field everywhere as a linear variation in the z direction:

$$T = T_0 - Gz \tag{5}$$

where T_0 is a reference temperature which locates the origin of the moving coordinate system relative to the solidification front, and G is the temperature gradient.

The presence of the eutectic on the phase diagram means that the liquid domain does not extend to $z = \infty$. We assume that once the eutectic temperature is reached the remaining liquid solidifies as the eutectic phase. Thus, the vertical coordinate at which the eutectic transformation occurs is given by

$$z_E = (T_0 - T_E)/G \tag{6}$$

and effectively truncates the liquid domain with the boundary condition

$$C = C_E \quad \text{at } z = z_E \text{ in } \mathscr{L} \tag{7}$$

where C_E is the eutectic composition. In the analysis that follows, we shall assume that C_∞ is not too close to C_E (in a sense to be quantified later).

We seek a steady-state solution to the free boundary problem posed by equations (1)–(7) in the form of a regular array of identical needle crystals (see Fig. 1). For definiteness we take the array to have a rectangular planform with spacings λ_x and λ_y; the center line of each crystal in the array is located at $(x, y) = (i\lambda_x, j\lambda_y)$, where i and j each range over all the integers. In principle it should also be possible to consider other array planforms such as hexagons.

In addition to the array spacings, there are two other length scales which specify the array morphology. The first is the tip position z_{tip}, which locates the vertical coordinate of the tips relative to the origin. Since the temperature gradient is linear, z_{tip} translates directly to a tip temperature (or tip undercooling). The second length scale is the tip radius ρ, which is related to the two principal radii of curvature at the tip, ρ_1 and ρ_2, by $2/\rho = 1/\rho_1 + 1/\rho_2$. We want to determine how the morphology length scales λ_x, λ_y, z_{tip}, and ρ vary in response to the material and control parameters.

We nondimensionalize the system as follows. We choose the reference temperature T_0 as the liquidus temperature at $C = C_\infty$:

$$T_0 = T_M + m_L C_\infty. \tag{8}$$

Since we expect the rejection of solute to elevate the liquid concentration at the tip relative to the mean alloy composition, the phase diagram, together with equation (5), indicates that the tips will lie in $z > 0$. From the phase diagram we also note a characteristic temperature scale ΔT_0 as the equilibrium freezing range at composition C_∞, given by

$$\Delta T_0 = m_L(k - 1)C_\infty/k. \tag{9}$$

From the control variables and material properties, one can define three fundamental process lengths [5]: the diffusion length $l_D = D/V$; the thermal length $l_T = k\,\Delta T_0/G$; and the capillary length $l_C = \Gamma/(k\,\Delta T_0)$. We nondimensionalize (x, y, z) with l_D, and nondimensionalize time with D^2/V to obtain

$$\frac{\partial C^*}{\partial t^*} = \nabla^2 C^* - \frac{\partial C^*}{\partial z^*} \quad \text{in } \mathscr{L} \tag{10}$$

$$C^* = (l_D/l_T)z^* - (l_C/l_D)\kappa^* \quad \text{on } \mathscr{B} \tag{11}$$

$$(V_n^* - n_z)[1 + C^*(1 - k)] + (\mathbf{n} \cdot \nabla C^*) = 0 \quad \text{on } \mathscr{B} \tag{12}$$

$$C^* \to 0 \quad \text{as } z^* \to -\infty \tag{13}$$

and

$$C^* = (C_E/C_\infty - 1)/(1 - k) \quad \text{at } z^* = Z_E^* \text{ in } \mathscr{L}. \tag{14}$$

In the above, starred quantities denote appropriately nondimensionalized variables where $C^* = (C - C_\infty)/[C_\infty(1 - k)]$ and $z_E^* = (l_T/l_D)(C_E/C_\infty - 1)/(1 - k)$. The system has four nondimensional control/material parameters: k; l_D/l_T; l_C/l_D; and C_E/C_∞. In addition, there are four nondimensional parameters describing the morphology of the array: ρ/l_D; λ_x/l_D; λ_y/l_D; and z_{tip}/l_D. The quantity ρ/l_D is the Peclet number of the dendrite tip†. Equations (10)–(14) represent the free boundary problem we need to solve.

3. LENGTH SCALE ANALYSIS

We want to determine how the morphology length scales vary in response to the control length scales. If all the nondimensional parameters are of order unity, the free boundary problem must be solved numerically. Our approach will be to develop simpler asymptotic solutions to the problem when one or more of the parameters is small. We choose our small parameters and scalings carefully by considering the size of the nondimensional parameters that are characteristic of dendtritic growth.

We develop our asymptotic scalings by considering the experiments of Somboonsuk, Mason and Trivedi (SMT) [7] on the directional solidification of a binary mixture of succinonitrile-acetone. The experimental apparatus consists of two closely spaced parallel plates with spacing Δy. For the experimental conditions considered, the array of dendrites formed a single row between the plates. Thus, the plate configuration effectively sets one of the dendrite spacings, $\lambda_y = \Delta y$. A further discussion can be found in Warren and Langer [8]. In the experiments, the

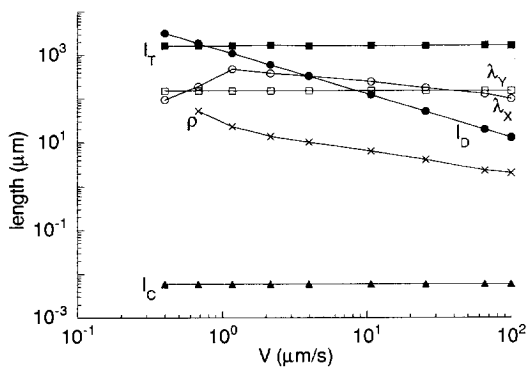

Fig. 3. Log–log plot of fundamental length scales as a function of growth velocity for the Somboonsuk *et al.* experiments [7]. The cell-to-dendrite transition occurs at about $V = 1$ μm/s. We base our observations of scale separation on the data at $V \approx 10$ μm/s.

†Note that our definition of l_D differs by a factor of 2 from that often used to describe dendritic growth. Thus our Peclet number differs by a factor of 2 from the traditional notation. The ratios l_{PD}/l_{PT} and l_C/l_D also differ by a factor of 2 from the parameters $\mathscr{G}$ and $\mathscr{A}$ of Trivedi [6].

composition C_∞ was held constant while V and G were varied. The experimental results include measurements of ρ and λ_x.

We plot the control and morphological length scales as a function of growth velocity V in Fig. 3. Since the tip undercooling was not reported in the experiments, the corresponding value of z_{tip} is not plotted. From the data on length scales we observe that, away from the cell-to-dendrite transition at about $V = 1$ μm/s, there is a separation of scales with

$$l_C \ll \rho \ll l_D \ll l_T. \tag{15}$$

Further, over a wide range of velocities, the dendrite spacings and diffusion length are of the same order of magnitude. We interpret this correlation to give the scaling

$$\lambda_x, \lambda_y = \text{ord}(l_D) \tag{16}$$

where the notation "ord" denotes "the same order as" as described in Ref. [9]. These observations form the basis for constructing a set of scalings for the nondimensional parameters. A unique set of scalings can be obtained by assuming that the resulting morphological lengths for the array obey the two scaling relationships presented in Ref. [5] for dendritic growth during directional solidification. These additional relationships are

$$\rho \propto l_D^{1/2} l_C^{1/2} \tag{17}$$

and

$$\lambda \propto l_T^{1/2} l_D^{1/4} l_C^{1/4}. \tag{18}$$

Finally, we assume that the alloy composition is not close to the eutectic composition in the sense that C_E^* is order (1).

We define a fundamental nondimensional parameter ϵ as the ratio of the diffusion length to the thermal length:

$$\epsilon = l_D/l_T. \tag{19}$$

It thus follows from the separation of scales [equation (15)] that ϵ is small:

$$\epsilon \ll 1. \tag{20}$$

Then, from a combination of equations (15)–(18) we obtain the following scalings for the nondimensional parameters:

$$(\lambda_x, \lambda_y)/l_D = (\Lambda_x, \Lambda_y) \tag{21}$$

$$\rho/l_D = \epsilon P \tag{22}$$

and

$$l_C/l_D = \epsilon^2 \Omega \tag{23}$$

where Λ_x, Λ_y, P, and Ω are all ord(1) nondimensional parameters. While no information about the appropriate scaling for z_{tip}/l_D can be inferred from the experiments, we can determine a consistent scaling by considering the behavior of an Ivantsov dendrite [1] growing into a supersaturated solution at uniform temperature. The scaling equation (22) means that the Peclet number of the tip is ord(ϵ). For the Ivantsov dendrite to have a Peclet number of ord(ϵ), the nondimensional undercooling $(C_{tip} - C_\infty)/[C_{tip}(1-k)]$ must be ord[$\epsilon \ln(1/\epsilon)$]. Taking C_{tip} on the liquidus isotherm, one finds that the tip position must necessarily scale as $z_{tip}/l_D = \text{ord}[\ln(1/\epsilon)]$. We thus define

$$z_{tip}/l_D = \mathscr{Z} \ln(1/\epsilon) \tag{24}$$

where $\mathscr{Z} = \text{ord}(1)$.

We are now in a position to derive an asymptotic solution to the free boundary problem in terms of the small parameter ϵ. In terms of the physical parameters,

$$\epsilon = \frac{l_D}{l_T} = \frac{DG}{Vm_L(k-1)C_\infty}. \tag{25}$$

The parameter ϵ measures the stabilizing effect of the temperature gradient relative to the destabilizing effect of the solute boundary layer. For morphological instability of an initially planar solidification front, it is necessary that [10]

$$\frac{Vm_L C_\infty (k-1)}{kDG} > 1 \tag{26}$$

which corresponds to $\epsilon < 1/k$. Thus $\epsilon \ll 1$ is a consistent parameter choice to describe dendritic morphologies. For the SMT experiments, $\epsilon < 0.1$ except for velocities near the cell-to-dendrite transition.

4. SOLUTION BY MATCHED ASYMPTOTIC EXPANSIONS

We now look for steady-state solutions to the free boundary problem in equations (10)–(14) using the scalings presented in Section 2. Dropping the stars from the nondimensional variables as a notational convenience, we obtain the following equations for a steady-state array:

$$\nabla^2 C - \frac{\partial C}{\partial z} = 0 \quad \text{in } \mathscr{L} \tag{27}$$

$$C = \epsilon z - \epsilon^2 \Omega \kappa \quad \text{on } \mathscr{B} \tag{28}$$

$$-n_z(1 + (1-k)C) + (\mathbf{n} \cdot \nabla C) = 0 \quad \text{on } \mathscr{B} \tag{29}$$

$$C \to 0 \quad \text{as } z \to -\infty \tag{30}$$

and

$$C = (C_E/C_\infty - 1)/(1-k) \quad \text{at } z = (1/\epsilon)(C_E/C_\infty - 1)/(1-k) \quad \text{in } \mathscr{L}. \tag{31}$$

For the rest of the paper we shall be concerned with these scaled variables and equations. We seek the solution to this nonlinear free boundary problem as an array of needle crystal dendrites. The array morphology is characterized by scaled parameters corresponding to the tip position $\mathscr{Z}$, the tip radius P, and the array spacings Λ_x and Λ_y.

Since we are looking for array solutions in which all dendrites are identical, we are free to describe the array relative to a particular "center" dendrite. In our solution we shall focus on a particular dendrite and how it behaves in the array. We denote the radial coordinate r as the distance from the center-axis of the center dendrite (see Fig. 4). The shape of the center dendrite can thus be described in terms of cylindrical coordinates by $r = R(\theta, z)$.

We solve the free boundary problem using matched asymptotic expansions (see also Refs [11] and [12] for applications of matched asymptotic expansions for dendritic growth of single component materials). There are four distinct asymptotic regions (see Fig. 4) for the solute field near the center dendrite. The four regions are

- Tip region: $r = O(\epsilon)$ and $z - z_{tip} = O(\epsilon)$
- Inner region: $r = O(\epsilon^{1/2})$ and $z - z_{tip} = O(1)$ with $z - z_{tip} > 0$
- Outer region: $r = O(1)$ and $z - z_{tip} = O(1)$
- Tail region: $r = O(1)$ and $z - z_{tip} = O(1/\epsilon)$ with $z - z_{tip} > 0$.

We shall solve the governing equations in each of the four asymptotic regions to obtain four locally valid solutions. Then, by requiring the solutions to match in the relevant overlap regions, we generate a uniformly valid solution to the free boundary problem. The following subsections detail the solutions in each region and the matching of solutions. (A reader interested in the conclusions but not necessarily the details might now turn to Section 4.9.)

4.1. *Inner solution*

In the inner region $r = O(\epsilon^{1/2})$ and $z - z_{tip} = O(1)$ with $z - z_{tip} > 0$. Relative to this local region, the neighboring dendrites in the array appear far away. The composite effect of the individual neighbors becomes a far-field matching condition on the inner solution.

For the inner region we use cylindrical coordinates $(\bar{r}, \theta, \zeta)$ where $\bar{r}$ is a scaled radial coordinate given by

$$\bar{r} = \frac{r}{\epsilon^{1/2}} \tag{32}$$

θ is the azimuthal angle, and ζ is the vertical coordinate measuring the distance along the dendrite from the dendrite tip:

$$\zeta = z - z_{tip}. \tag{33}$$

In the inner region $\zeta > 0$. For a roughly parabolic dendrite with an $O(\epsilon)$ Peclet number, the scaled dendrite shape $\bar{r} = \bar{R}(\theta, \zeta)$ must be given by

$$\bar{R}(\theta, \zeta) = \frac{R(\theta, z)}{\epsilon^{1/2}} \tag{34}$$

from which it follows that the curvature $\bar{\kappa}$ in inner variables is given by

$$\bar{\kappa} = \epsilon^{1/2}\kappa. \tag{35}$$

Balancing the magnitude of the largest terms in the concentration boundary condition (28), we find the scaling for the inner concentration field $\bar{C}$ must be

$$\bar{C}(\bar{r}, \theta, \zeta) = \frac{\delta}{\epsilon} C(r, \theta, z) \tag{36}$$

where $\delta \equiv 1/\ln(1/\epsilon)$. We substitute the inner scalings (32)–(36) into the governing equations (27)–(29). Equations (30) and (31) are not relevant to the inner region. The equations for the inner region are

$$\frac{1}{\bar{r}}\frac{\partial}{\partial \bar{r}}\left(\bar{r}\frac{\partial \bar{C}}{\partial \bar{r}}\right) + \frac{1}{\bar{r}^2}\frac{\partial^2 \bar{C}}{\partial \theta^2} + \epsilon\left(\frac{\partial^2 \bar{C}}{\partial \zeta^2} - \frac{\partial \bar{C}}{\partial \zeta}\right) = 0 \quad \text{in } \bar{r} > \bar{R}(\theta, \zeta) \tag{37}$$

$$\bar{C} = \mathscr{L} + \delta\zeta - \delta\epsilon^{1/2}\Omega\bar{\kappa} \quad \text{on } \bar{r} = \bar{R}(\theta, \zeta) \tag{38}$$

and

$$\frac{\partial \bar{C}}{\partial \bar{r}} - \frac{1}{\bar{R}^2}\frac{\partial \bar{C}}{\partial \theta}\frac{\partial \bar{R}}{\partial \theta} + \delta\frac{\partial \bar{R}}{\partial \zeta} + \epsilon\frac{\partial \bar{R}}{\partial \zeta}\left((1-k)\bar{C} - \frac{\partial \bar{C}}{\partial \zeta}\right) = 0 \quad \text{on } \bar{r} = \bar{R}(\theta, \zeta). \tag{39}$$

In addition to these equations, the inner solution must also satisfy matching conditions with the solutions from the other regions. We will first find a solution to the inner equations above, and then make the solution match the other solutions in subsequent sections.

We seek a solution to the system of inner equations as an expansion in the small parameters $\delta = 1/\ln(1/\epsilon)$ and ϵ. Since δ is only "logarithmically" small with

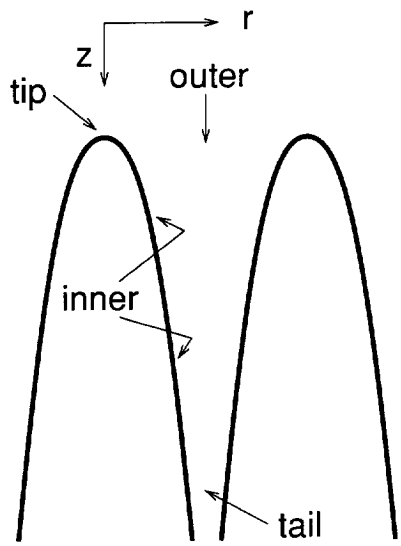

Fig. 4. Schematic of different asymptotic regions employed in the solution by matched asymptotic expansions.

respect to ϵ, it follows that all terms of the form δ^n are necessarily much larger than all terms of the form ϵ^m (for $n, m > 0$). Thus, a power series expansion in δ and ϵ will start out as

$$\bar{C} = \bar{C}_0 + \delta\bar{C}_1 + \delta^2\bar{C}_2 + \cdots + \text{“}\epsilon \text{ terms”} \tag{40}$$

where “ϵ terms” represent all terms in the expansion containing a factor of the form ϵ^m, $m > 0$. Our aim in this paper will be to obtain a solution for the first part of this expansion—the δ^n terms. Since the δ^n terms are formally larger than all the ϵ^m terms, we can ignore the “ϵ terms” in determining the δ^n expansion. In principle there is nothing to prevent one from using our results from the δ-expansion to determine the higher-order ϵ terms in the expansion.

We now determine the δ-expansion given by the first line of equation (40). Dropping the ϵ terms from the inner equations (37)–(39), we obtain

$$\frac{1}{\bar{r}}\frac{\partial}{\partial\bar{r}}\left(\bar{r}\frac{\partial\bar{C}}{\partial\bar{r}}\right) + \frac{1}{\bar{r}^2}\frac{\partial^2\bar{C}}{\partial\theta^2} = 0 \quad \text{in } \bar{r} > \bar{R}(\theta, \zeta) \tag{41}$$

$$\bar{C} = \mathscr{Z} + \delta\zeta \quad \text{on } \bar{r} = \bar{R}(\theta, \zeta) \tag{42}$$

and

$$\frac{\partial\bar{C}}{\partial\bar{r}} - \frac{1}{\bar{R}^2}\frac{\partial\bar{C}}{\partial\theta}\frac{\partial\bar{R}}{\partial\theta} + \delta\frac{\partial\bar{R}}{\partial\zeta} = 0 \quad \text{on } \bar{r} = \bar{R}(\theta, \zeta). \tag{43}$$

The small parameter δ appearing in the above equations is only “logarithmically” small; the numerical value of δ for the SMT experiments is in the range $0.2 < \delta < 2.5$ for dendritic growth. The relatively large size of δ means that the straightforward asymptotic expansion in powers of δ may require many terms to give a good approximation to the solution. In order to get around the slow convergence of the δ-series we shall solve the inner equations *exactly* for arbitrary δ. The solution we obtain is the *summation of all the δ terms* in the expansion (40).

We look for an inner solution which is axisymmetric to all orders in δ. The axisymmetric solution to equation (41) is

$$\bar{C} = A(\zeta)\ln\bar{r} + B(\zeta) \tag{44}$$

where $A(\zeta)$ and $B(\zeta)$ are arbitrary functions of ζ. We substitute this solution into the boundary condition (42) to find

$$B(\zeta) = \mathscr{Z} + \delta\zeta - A(\zeta)\ln\bar{R}(\zeta). \tag{45}$$

From the second boundary condition [equation (43)] we obtain

$$\frac{A(\zeta)}{\bar{R}(\zeta)} + \delta\frac{\mathrm{d}\bar{R}}{\mathrm{d}\zeta} = 0 \tag{46}$$

which can be integrated to give

$$(1/2)\bar{R}^2 = \frac{-1}{\delta}\int_0^\zeta A(\zeta')\,\mathrm{d}\zeta' \tag{47}$$

where we have chosen the integration constant so that $\bar{R} = 0$ at the dendrite tip $\zeta = 0$. Thus the inner solution, valid for arbitrary δ (but neglecting ϵ terms), is given by

$$\bar{C} = A(\zeta)\ln(\bar{r}/\bar{R}) + \mathscr{Z} + \delta\zeta \tag{48}$$

where $A(\zeta)$ is an unknown function to be determined by matching to the outer solution.

4.2. *Outer solution*

In the outer region, $r = O(1)$ and $z - z_{\text{tip}} = O(1)$. On the scale of the outer region (see Fig. 4) the dendrites appear as an array of line sources at $x = i\Lambda_x$, $y = j\Lambda_y$, extending from $z = z_{\text{tip}}$ to $z = \infty$.

For the outer region we use a Cartesian coordinate system (x, y, ζ) with the origin located at the tip of the center dendrite, with $\zeta = z - z_{\text{tip}}$. The concentration in the outer region C_{out} must match with that of the inner region in an intermediate overlap region. To achieve this matching, C_{out} must be related to the unscaled concentration field C by

$$C_{\text{out}}(x, y, \zeta) = \frac{\delta}{\epsilon}C(x, y, z). \tag{49}$$

We substitute the outer scalings into the governing equations (27) and (30), the only equations relevant to the outer region. The resulting outer equations are

$$\nabla^2 C_{\text{out}} - \frac{\partial C_{\text{out}}}{\partial z} = 0 \quad \text{in } \mathscr{L} \tag{50}$$

and

$$C_{\text{out}} \to 0 \quad \text{as } \zeta \to -\infty. \tag{51}$$

In addition, the outer solution must match the solutions from the other asymptotic regions.

The outer solution can be written in terms of an array of line sources:

$$C_{\text{out}} = \sum_{i=-\infty}^{\infty}\sum_{j=-\infty}^{\infty}\int_0^\infty q(\zeta')G_{ij}(x, y, \zeta; \zeta')\,\mathrm{d}\zeta'. \tag{52}$$

In the above expression $q(\zeta)$ is the strength of the vertical line source for each dendrite, the indices i and j denote the individual dendrites in the array, the summation is a sum over all the dendrites in the array, and G_{ij} is related to the Green's function for the advection–diffusion equation, with

$$G_{ij}(x, y, \zeta; \zeta') = \frac{1}{4\pi}\frac{\exp\{-(1/2)[\sqrt{(x - i\Lambda_x)^2 + (y - j\Lambda_y)^2 + (\zeta' - \zeta)^2} + (\zeta' - \zeta)]\}}{\sqrt{(x - i\Lambda_x)^2 + (y - j\Lambda_y)^2 + (\zeta' - \zeta)^2}}. \tag{53}$$

The Green's function G_{ij} measures the response at (x, y, ζ) to a concentration source at vertical position ζ' on the line source at $x = i\Lambda_x$ and $y = j\Lambda_y$. The source strength $q(\zeta)$ is an unknown function which is to be determined by matching to the solutions in the tip, inner, and tail regions.

4.3. Matching inner and outer solutions

The inner and outer solutions must match asymptotically in an intermediate "overlap" region. The intermediate region for the inner and outer solution is given by $\epsilon^{1/2} \ll r \ll 1$ and $\zeta = O(1)$ with $\zeta > 0$. We introduce the intermediate variable

$$\tilde{r} = \frac{r}{\epsilon^{\alpha/2}} \tag{54}$$

where $0 < \alpha < 1$, and seek matching solutions for arbitrary α. The inner solution is given in terms of intermediate variables as

$$\bar{C} = \frac{(1-\alpha)}{2\delta} A(\zeta) + A(\zeta)\ln\frac{\tilde{r}}{\bar{R}} + \mathscr{Z} + \delta\zeta \tag{55}$$

where we have made use of $\delta = 1/\ln(1/\epsilon)$. To expand the outer solution in the intermediate region, we separate C_{out} into two pieces:

$$C_{out} = C_{near} + C_{array} \tag{56}$$

where C_{near} is the contribution to the solute field made by the "center" line source and C_{array} is the contribution made by the rest of the line sources in the array. Thus

$$C_{near} = \int_0^\infty q(\zeta')G_{00}(x, y, \zeta; \zeta')\,d\zeta' \tag{57}$$

and

$$C_{array} = \sum_{i^2+j^2\neq 0}\sum \int_0^\infty q(\zeta')G_{ij}(x, y, \zeta; \zeta')\,d\zeta'. \tag{58}$$

From an asymptotic analysis of C_{near} in the intermediate region, we find that

$$C_{near} = \frac{\alpha q(\zeta)}{4\pi\,\delta} - \frac{q(\zeta)}{4\pi}\left[\ln\left(\frac{\tilde{r}^2}{4\zeta}\right) + \gamma_E\right] + \int_0^\infty [q(\zeta') - q(\zeta)]G_{near}(\zeta; \zeta')\,d\zeta' + \text{"}\epsilon \text{ terms"}. \tag{59}$$

In the above equation, γ_E is Euler's constant, G_{near} is given by

$$G_{near}(\zeta; \zeta') = \frac{1}{4\pi}\frac{\exp\{-(1/2)[|\zeta' - \zeta| + (\zeta' - \zeta)]\}}{|\zeta' - \zeta|} \tag{60}$$

and "ϵ terms" are terms that contain factors of the form ϵ^m $(m > 0)$, and thus do not enter into the matching process for the δ-expansion. An asymptotic expansion of C_{array} in the intermediate region gives

$$C_{array} = \int_0^\infty q(\zeta')G_{array}(\zeta; \zeta')d\zeta' + \text{"}\epsilon \text{ terms"} \tag{61}$$

where

$$G_{array}(\zeta; \zeta') = \sum_{i^2+j^2\neq 0}\sum \frac{1}{4\pi}\frac{\exp\{-(1/2)[\sqrt{(i\Lambda_x)^2 + (j\Lambda_x)^2 + (\zeta' - \zeta)^2} + (\zeta' - \zeta)]\}}{\sqrt{(i\Lambda_x)^2 + (j\Lambda_y)^2 + (\zeta' - \zeta)^2}}. \tag{62}$$

Thus, the outer solution in the intermediate region is given by

$$C_{out} = \frac{\alpha q(\zeta)}{4\pi\,\delta} - \frac{q(\zeta)}{4\pi}\left[\ln\left(\frac{\tilde{r}^2}{4\zeta}\right) + \gamma_E\right] + \int_0^\infty [q(\zeta') - q(\zeta)]G_{near}(\zeta; \zeta')\,d\zeta' + \int_0^\infty q(\zeta')G_{array}(\zeta; \zeta')\,d\zeta' + \text{"}\epsilon \text{ terms"}. \tag{63}$$

We now match $\bar{C}$ to C_{out} in the arbitrary overlap region (artibrary α) to all orders in δ. Dropping "ϵ terms" we have

$$\frac{(1-\alpha)}{2\,\delta} A(\zeta) + A(\zeta)\ln\left(\frac{\tilde{r}}{\bar{R}}\right) + \mathscr{Z} + \delta\zeta = \frac{\alpha q(\zeta)}{4\pi\,\delta} - \frac{q(\zeta)}{4\pi}\left[\ln\left(\frac{\tilde{r}^2}{4\zeta}\right) + \gamma_E\right] + \int_0^\infty [q(\zeta') - q(\zeta)]G_{near}(\zeta; \zeta')\,d\zeta' + \int_0^\infty q(\zeta')G_{array}(\zeta; \zeta')\,d\zeta'. \tag{64}$$

Matching for arbitrary α requires the α terms in equation (64) to vanish. Thus, the inner function $A(\zeta)$ and the outer function $q(\zeta)$ are related by

$$A(\zeta) = \frac{-1}{2\pi}q(\zeta). \tag{65}$$

We substitute this relationship into the matching

equation (64) to find an equation for the unknown source strength $q(\zeta)$:

$$\mathscr{L} + \delta\zeta = \frac{q(\zeta)}{4\pi\,\delta} - \frac{q(\zeta)}{4\pi}\left[\ln\left(\frac{\bar{R}^2}{4\zeta}\right) + \gamma_E\right] + \int_0^\infty [q(\zeta') - q(\zeta)]G_{near}(\zeta;\zeta')\,d\zeta' + \int_0^\infty q(\zeta')G_{array}(\zeta;\zeta')\,d\zeta'. \quad (66)$$

From relations (47) and (65) we also know the shape of the inner solution in terms of $q(\zeta)$:

$$[\bar{R}(\zeta)]^2 = \frac{1}{\pi\,\delta}\int_0^\zeta q(\zeta')\,d\zeta'. \quad (67)$$

The coupled system of equations (66) and (67) is the central result of our analysis. By solving the system for $q(\zeta)$ and $\bar{R}(\zeta)$ we determine the solution to the free boundary problem which matches the inner and outer solutions. The remaining asymptotic analysis describes the solution in the tip and tail regions, and how the tip and tail solutions match with the inner and outer solutions.

4.4. *Tip region*

In the tip region $r = O(\epsilon)$ and $z - z_{tip} = O(\epsilon)$. Relative to this local region, the tip appears as an isolated dendrite with an undercooling determined by the effect of the rest of the array. We denote the scaled tip region variables by tildes and use cylindrical coordinates $(\tilde{r}, \theta, \tilde{z})$ with $\tilde{r}$ and $\tilde{z}$ given by

$$\tilde{r} = \frac{1}{\epsilon}r \quad (68)$$

and

$$\tilde{z} = \frac{z - z_{tip}}{\epsilon}. \quad (69)$$

The associated scaled variables for the tip region are

$$\tilde{C}(\tilde{r}, \theta, \tilde{z}) = \frac{\delta}{\epsilon}C(x, y, z) \quad (70)$$

$$\tilde{R}(\theta, \tilde{z}) = \frac{1}{\epsilon}R(\theta, z) \quad (71)$$

$$\tilde{\kappa} = \epsilon\kappa \quad (72)$$

and

$$\mathscr{L} = \delta z_{tip}. \quad (73)$$

Upon substitution of the scalings into the governing equations, the tip equations are found to be

$$\nabla^2\tilde{C} - \epsilon\frac{\partial\tilde{C}}{\partial\tilde{z}} = 0 \quad \text{in } \mathscr{L} \quad (74)$$

$$\tilde{C} = \mathscr{L} - \delta\Omega\tilde{\kappa} + \epsilon\delta\tilde{z} \quad \text{on } \mathscr{B} \quad (75)$$

and

$$-n_z[\delta + \epsilon(1-k)\tilde{C}] + (\mathbf{n}\cdot\nabla\tilde{C}) = 0 \quad \text{on } \mathscr{B}. \quad (76)$$

Following the approach of Section 4.1, we construct a solution to the free boundary problem using an expansion in δ and ϵ, where we neglect "ϵ terms" and solve the remaining problem for arbitrary δ. In general, the full solution for the tip shape is not axially symmetric because of the periodic arrangement of neighboring dendrites in the array. At leading order, however, these asymmetries are not present because the dimension of the tip is relatively small compared to the scale of the dendrite spacing. We expect that the tip is axisymmetric to all orders in δ, and that departures from axisymmetry appear only as a higher-order ϵ term.

We drop the ϵ terms from the axisymmetric tip equations to obtain the following tip problem:

$$\nabla^2\tilde{C} = 0 \quad \text{in } \mathscr{L} \quad (77)$$

$$\tilde{C} = \mathscr{L} - \delta\Omega\tilde{\kappa} \quad \text{on } \mathscr{B} \quad (78)$$

and

$$(\mathbf{n}\cdot\nabla\tilde{C}) - \delta n_z = 0 \quad \text{on } \mathscr{B}. \quad (79)$$

The tip equations (77)–(79) represent a nonlinear free boundary problem for the tip shape. The equations are similar to those obtained for the isolated thermal dendrite, the difference being that here we do not have an advective term in the diffusion equation (77).

The presence of the Ω term in equation (78) has important implications for finding tip solutions. In the past, the surface energy term Ω has been identified as the physical effect that results in the selection of a unique tip radius for the isolated dendrite [13–16]. We suggest here that in the growth of alloy dendrite arrays the selection of the tip radius is not necessarily determined by the surface energy. We shall claim that, without the need for surface energy, there is a unique tip radius which depends on the spacing of the array. In what follows we shall illustrate this idea by considering the special case of $\Omega = 0$. Choosing $\Omega = 0$ is equivalent to saying that surface energy is negligible at the tip to first approximation. This choice can be made rigorous by revising our original scaling in equation (23). Instead of choosing $l_C/l_D = \epsilon^2\Omega$, we can consider the case where $l_C/l_D \ll \epsilon^2$. Given the wide disparity between l_C and l_D in Fig. 3, this new scaling is not necessarily inappropriate for dendritic growth at low-to-moderate velocities. With the revised scaling for l_C/l_D the surface energy term does not appear in the leading order problem for the tip and the effect of surface energy on the solutions will only enter at higher order. We plan to determine the effect of surface energy in future work. For now, we have taken $\Omega = 0$ ($l_C \ll \epsilon^2 l_D$) because it allows us to obtain a straightforward closed-form solution for the tip, enabling us to easily match the other solutions. Our choice of $\Omega = 0$ also serves to emphasize that it is

possible for the tip radius to be selected by the array spacing rather than by surface energy.

Taking $\Omega = 0$, we solve the tip region equations in paraboloidal coordinates (η, ξ, θ), where

$$\eta = (1/2)[\sqrt{\tilde{r}^2 + (\tilde{z} - \eta_*)^2} - (\tilde{z} - \eta_*)] \quad (80)$$

$$\xi = (1/2)[\sqrt{\tilde{r}^2 + (\tilde{z} - \eta_*)^2} + (\tilde{z} - \eta_*)] \quad (81)$$

and where $\eta*$ is the distance between the dendrite tip and the origin of the paraboloidal coordinate system located inside the dendrite. The tip equations become

$$\eta \frac{\partial^2 \tilde{C}}{\partial \eta^2} + \xi \frac{\partial^2 \tilde{C}}{\partial \xi^2} + \frac{\partial \tilde{C}}{\partial \eta} + \frac{\partial \tilde{C}}{\partial \xi} = 0 \quad \text{in} \quad \mathscr{L} \quad (82)$$

$$\tilde{C} = \mathscr{Z} \quad \text{on} \quad \eta = N(\xi) \quad (83)$$

and

$$N \frac{\partial \tilde{C}}{\partial \eta} - \xi \frac{\partial \tilde{C}}{\partial \xi} \frac{dN}{d\xi} + \delta \left[N + \xi \frac{dN}{d\xi} \right] = 0$$

$$\text{on } \eta = N(\xi). \quad (84)$$

We note that equation (82) has the solution

$$\tilde{C} = \tilde{A} \ln \eta + \tilde{B} \quad (85)$$

where $\tilde{A}$ and $\tilde{B}$ are constants. We seek a solution for the shape of the tip as

$$N(\xi) = \eta_*. \quad (86)$$

Substituting equations (85) and (86) into the boundary conditions (83) and (84), we obtain two equations for the constants $\tilde{A}$ and $\tilde{B}$. The solution of these equations is

$$\tilde{A} = -\delta \eta_* \quad (87)$$

and

$$\tilde{B} = \mathscr{Z} + \delta \eta_* \ln \eta_*. \quad (88)$$

From the curvature at the tip, one finds $\eta_* = P/2$, where P is the scaled Peclet number of the tip.

Incorporating equations (87) and (88) into equation (85), we determine that the tip solution is given by

$$\tilde{C}(\eta, \xi) = -\delta(P/2) \ln\left(\frac{\eta}{P/2}\right) + \mathscr{Z} \quad (89)$$

and

$$N(\xi) = P/2. \quad (90)$$

The constant P is to be determined by matching to the inner and outer solutions.

4.5. Matching tip and outer solutions

We match the tip and outer solutions in an intermediate overlap region where $\epsilon \ll r \ll 1$ and $\epsilon \ll |z - z_{tip}| \ll 1$. We introduce coordinates for the intermediate region as r_0 and z_0, where

$$r = \epsilon^{\alpha} r_0 \quad (91)$$

and

$$z = z_{tip} + \epsilon^{\beta} z_0. \quad (92)$$

In the above equations, the exponents α and β are arbitrary except for the restrictions that (i) $0 < \alpha < 1$, (ii) $0 < \beta < 1$, and (iii) $\beta \geq 2\alpha - 1$. The first two restrictions are necessary for the intermediate region to lie between the inner and outer regions. The last restriction follows from requiring the matching region to lie outside the dendrite.

In the intermediate region described above, the tip solution is given by

$$\tilde{C} = (v - 1)(P/2) + \mathscr{Z} + \delta(P/2)\ln(P/2) - \delta(P/2)\ln F(r_0, z_0) + O(\epsilon^{\tau}) \quad (93)$$

where the function $F(r_0, z_0)$ and the constants v and τ depend on the relative sizes of α and β. There are four cases; the results for each case are summarized in Table 1.

A representation for the outer solution [equation (52)] in the intermediate region may be found by writing

$$C_{out} = C_{near} + C_{array} \quad (94)$$

where C_{near} is the concentration field generated by the "center" line source and C_{array} is the concentration field generated by the rest of the dendrites in the array. After adding and subtracting the near-singularity at $\zeta' = 0$ in C_{near}, an asymptotic analysis of the integrals in the intermediate region gives

$$C_{near} = \frac{q(0)}{4\pi} E_1(\tilde{\eta}) + \int_0^{\infty} [q(\zeta') - q(0)] G_N^T(\zeta')\, d\zeta' + \text{“}\epsilon \text{ terms”} \quad (95)$$

where

$$\tilde{\eta} = (1/2)[\sqrt{r^2 + \zeta^2} - \zeta] \quad (96)$$

and

$$G_N^T(\zeta) = \frac{\exp(-\zeta)}{4\pi\zeta}. \quad (97)$$

Table 1. Four cases for matching tip to outer solution

Case	v	$F(r_0, z_0)$	τ
I. $\alpha = \beta$	α	$[(r_0^2 + z_0^2)^{1/2} - z_0]/2$	$1 - \alpha$
II. $\alpha < \beta$	α	$r_0/2$	$\beta - \alpha$
III. $\alpha > \beta$, $z_0 < 0$	β	$-z_0$	$1 - \beta$, $2(\alpha - \beta)$
IV. $\alpha > \beta$, $z_0 > 0$	$2\alpha - \beta$	$r_0^2/(4z_0)$	$2(1 - \alpha)$

Expanding C_{near} in intermediate variables, we obtain

$$C_{near} = \nu \frac{q(0)}{4\pi\,\delta} - \frac{q(0)}{4\pi}\,[\ln F(r_0, z_0) + \gamma_E] + \int_0^\infty [q(\zeta') - q(0)]G_N^T(\zeta')\,d\zeta' + \text{“}\epsilon \text{ terms”} \quad (98)$$

where ν and $F(r_0, z_0)$ are as given in Table 1. We expand C_{array} in the intermediate region to find

$$C_{array} = \int_0^\infty q(\zeta')G_A^T(\zeta')\,d\zeta' + \text{“}\epsilon \text{ terms”} \quad (99)$$

where

$$G_A^T(\zeta') = \sum_{i^2+j^2\neq 0}\sum \frac{1}{4\pi}\frac{\exp\{-(1/2)[\sqrt{(i\Lambda_x)^2 + (j\Lambda_y)^2 + (\zeta')^2} + \zeta']\}}{\sqrt{(i\Lambda_x)^2 + (j\Lambda_y)^2 + (\zeta')^2}}. \quad (100)$$

Thus, in the intermediate region,

$$C_{out} = \nu \frac{q(0)}{4\pi\,\delta} - \frac{q(0)}{4\pi}\,[\ln F(r_0, z_0) + \gamma_E] + \int_0^\infty [q(\zeta') - q(0)]G_N^T(\zeta')\,d\zeta' + \int_0^\infty q(\zeta')G_A^T(\zeta')d\zeta' + \text{“}\epsilon \text{ terms”}. \quad (101)$$

We now drop the “ϵ terms” and match $\tilde{C}$ to C_{out} for arbitrary α and β to all orders in δ. Matching requires the cancellation of terms with factors of ν, which gives

$$P = \frac{q(0)}{2\pi\delta}. \quad (102)$$

Thus the scaled Peclet number is linked directly to the source strength at the tip. Upon substitution of this relationship back into the matching condition, and after some rearranging, the matching condition becomes

$$\mathscr{Z} = \frac{q(0)}{4\pi\delta} - \frac{q(0)}{4\pi}\left[\ln\frac{q(0)}{4\pi\delta} + \gamma_E\right] + \int_0^\infty [q(\zeta') - q(0)]G_N^T(\zeta')\,d\zeta' + \int_0^\infty q(\zeta')G_A^T(\zeta')\,d\zeta'. \quad (103)$$

A comparison of equation (103) to the matching condition (66) reveals that equation (103) is the limiting version of (66) as $\zeta \to 0$. Thus, solutions to the inner/outer matching condition (66) automatically satisfy the tip/outer matching condition (103). The only new information determined by matching the tip to the outer solution is the relation (102) between the scaled tip radius and the source strength at the dendrite tip.

4.6. Matching tip and inner solutions

We match the tip and inner solutions in an intermediate region where $\epsilon \ll r \ll \epsilon^{1/2}$ and $\epsilon \ll |z - z_{tip}| \ll 1$ with $z - z_{tip} > 0$. We introduce coordinates for the intermediate region as r_* and z_*, where

$$r = \epsilon^\alpha r_* \quad (104)$$

and

$$z = z_{tip} + \epsilon^\beta z_*. \quad (105)$$

In the above equations, the exponents α and β are arbitrary constants except for the restrictions: (i) $1/2 < \alpha < 1$; (ii) $0 < \beta < 1$; (iii) $\beta \geqslant 2\alpha - 1$; and (iv) $\alpha > \beta$. Restrictions (i) and (ii) follow directly from the definition of the intermediate region. Restriction (iii) is necessary for the matching region to lie outside the dendrite. Restriction (iv) comes from considering the parabolic nature of the tip. In paraboloidal tip coordinates (ξ, η) [see equations (80)–(81)] we expect to match the tip solution to the inner solution as $\xi \to \infty$ for $\eta = O(1)$. To ensure that η remains $O(1)$ as the tip coordinates $\tilde{r} \to \infty$ and $\tilde{z} \to \infty$, we must require that $\tilde{r}/\tilde{z} \ll 1$, which translates to $\alpha > \beta$ in the intermediate region.

In the intermediate region the tip solution [equation (89)] is given by

$$\tilde{C} = (2\alpha - \beta - 1)(P/2) + \mathscr{Z} + \delta(P/2)\ln(P/2) - \delta(P/2)\ln(r_*^2/4z_*) + \text{“}\epsilon \text{ terms”}. \quad (106)$$

In the intermediate region the inner solution [equation (48)] is given by

$$\bar{C} = \frac{q(0)}{4\pi\,\delta}(2\alpha - \beta - 1) + \mathscr{Z} + \frac{q(0)}{4\pi}\ln\left(\frac{q(0)}{4\pi\,\delta}\right) - \frac{q(0)}{4\pi}\ln(r_*^2/4z_*) + \text{“}\epsilon \text{ terms”}. \quad (107)$$

The matching of $\tilde{C}$ to $\bar{C}$ for arbitrary α and β for all orders in δ can be guaranteed by choosing $P = q(0)/2\pi\delta$ as given by equation (102). Thus, matching of the tip and inner solutions automatically follows from the matching of inner-to-outer and tip-to-outer solutions. Our tip, inner, and outer solutions now match in all three overlap regions. All that remains is to account for the solution in the tail region and demonstrate that it matches the inner and outer solutions.

4.7. Tail solution

In the tail region $r = O(1)$ and $z = O(1/\epsilon)$. On the scale of the tail region, the dendrite trunk widens slowly along the length of the dendrite and fills the interdendrite region. We scale the vertical coordinate in the tail region as

$$z = z_v/\epsilon \tag{108}$$

where z_v is $O(1)$. All other nondimensional variables in the original equations (27)–(31) remain $O(1)$ in the tail region. We define $C_v(x, y, z_v) = C(x, y, z)$, $R_v(\theta, z_v) = R(\theta, z)$, and $\kappa_v(\theta, z_v) = \kappa(\theta, z)$, and substitute these along with the tail scaling of equation (108) into the unscaled system of equations (27)–(31) to obtain

$$\frac{\partial^2 C_v}{\partial x^2} + \frac{\partial^2 C_v}{\partial y^2} - \epsilon \frac{\partial C_v}{\partial z_v} + \frac{\partial^2 C_v}{\partial z_v^2} = 0 \quad \text{in } \mathscr{L} \tag{109}$$

$$C_v = z_v - \epsilon^2 \Omega \kappa_v \quad \text{on } r = R_v(\theta, z_v) \tag{110}$$

$$\frac{\partial C_v}{\partial r} - \frac{1}{R_v^2}\frac{\partial C_v}{\partial \theta}\frac{\partial R_v}{\partial \theta} + \epsilon \frac{\partial R_v}{\partial z_v}[1 + (1-k)C_v] - \epsilon^2 \frac{\partial R_v}{\partial z_v}\frac{\partial C_v}{\partial z_v} = 0 \quad \text{on } r = R_v(\theta, z_v) \tag{111}$$

and

$$C_v = (C_E/C_\infty - 1)/(1-k) \quad \text{at } z_v = (C_E/C_\infty - 1)/(1-k) \quad \text{in } \mathscr{L}. \tag{112}$$

In addition, the symmetry of the periodic array is equivalent to a no-flux condition on the boundaries of the periodic cell surrounding the center dendrite. Thus,

$$\mathbf{n}_{cell} \cdot \nabla C_v = 0 \quad \text{on } x = \pm \Lambda_x/2, \quad |y| \leqslant \Lambda_y/2 \quad \text{and } y = \pm \Lambda_y/2, \quad |x| \leqslant \Lambda_x/2 \tag{113}$$

where $\mathbf{n}_{cell}$ is the outward unit normal to the rectangular cell $|x| \leqslant \Lambda_x/2$, $\Lambda_y/|y| \leqslant 2$.

The system of equations (109)–(113) contains the small parameter ϵ but does not contain the parameter δ. Thus we can solve the tail system with an expansion in ϵ only. We let

$$C_v = C_0 + \epsilon C_1 + \cdots \tag{114}$$

and

$$R_v = R_0 + \epsilon R_1 + \cdots. \tag{115}$$

In order to match to our leading-order (δ-summed) solution for the inner and outer regions, we must determine the leading-order shape R_0 for the tail.

The $O(1)$ problem for the tail is

$$\frac{\partial^2 C_0}{\partial x^2} + \frac{\partial^2 C_0}{\partial y^2} = 0 \quad \text{in } \mathscr{L} \tag{116}$$

$$C_0 = z_v \quad \text{on } r = R_0(\theta, z_v) \tag{117}$$

$$\frac{\partial C_0}{\partial r} - \frac{1}{R_0^2}\frac{\partial C_0}{\partial \theta}\frac{\partial R_0}{\partial \theta} = 0 \quad \text{on } r = R_0(\theta, z_v) \tag{118}$$

$$C_0 = (C_E/C_\infty - 1)/(1-k) \quad \text{at } z_v = (C_E/C_\infty - 1)/(1-k) \quad \text{in } \mathscr{L} \tag{119}$$

and

$$\mathbf{n}_{cell} \cdot \nabla C_0 = 0 \quad \text{on } x = \pm \Lambda_x/2, \ |y| \leqslant \Lambda_y/2 \quad \text{and } y = \pm \Lambda_y/2, \ |x| \leqslant \Lambda_x/2. \tag{120}$$

The leading-order problem has a one-dimensional solution

$$C_0 = z_v \tag{121}$$

with R_0 undetermined at this order. To determine R_0 we proceed to $O(\epsilon)$.

The $O(\epsilon)$ problem for the tail is

$$\frac{\partial^2 C_1}{\partial x^2} + \frac{\partial^2 C_1}{\partial y^2} - \frac{\partial C_0}{\partial z_v} = 0 \quad \text{in } \mathscr{L} \tag{122}$$

$$C_1 = 0 \quad \text{on } r = R_0(\theta, z_v) \tag{123}$$

$$\frac{\partial C_1}{\partial r} - \frac{1}{R_0^2}\frac{\partial C_1}{\partial \theta}\frac{\partial R_0}{\partial \theta} + \frac{\partial R_0}{\partial z_v}[1 + (1-k)C_0] = 0 \quad \text{on } r = R_0(\theta, z_v) \tag{124}$$

$$C_1 = 0 \quad \text{at } z_v = (C_E/C_\infty - 1)/(1-k) \quad \text{in } \mathscr{L} \tag{125}$$

and

$$\mathbf{n}_{cell} \cdot \nabla C_1 = 0 \quad \text{on } x = \pm \Lambda_x/2, \ |y| \leqslant \Lambda_y/2 \quad \text{and } y = \pm \Lambda_y/2, \ |x| \leqslant \Lambda_x/2. \tag{126}$$

After substituting for the $O(1)$ solution C_0, the $O(\epsilon)$ equations can be rewritten as the following two-dimensional system in the variables x and y, where the vertical tail coordinate z_v appears as a time-like parameter:

$$\nabla_H^2 C_1 = 1 \quad \text{in } \mathscr{L} \tag{127}$$

$$C_1 = 0 \quad \text{on } r = R_0(\theta, z_v) \tag{128}$$

$$\sqrt{1 + \frac{1}{R_0^2}\left(\frac{\partial R_0}{\partial \theta}\right)^2}(\mathbf{n}_H \cdot \nabla_H C_1) + \frac{\partial R_0}{\partial z_v}[1 + (1-k)z_v] = 0 \quad \text{on } r = R_0(\theta, z_v) \tag{129}$$

$$C_1 = 0 \quad \text{at } z_v = (C_E/C_\infty - 1)/(1-k) \quad \text{in } \mathscr{L} \tag{130}$$

and

$$\mathbf{n}_{cell} \cdot \nabla_H C_1 = 0 \quad \text{on } x = \pm \Lambda_x/2, \ |y| \leqslant \Lambda_y/2 \quad \text{and } y = \pm \Lambda_y/2, \ |x| \leqslant \Lambda_x/2. \tag{131}$$

In the above equations ∇_H is the (horizontal) two-dimensional gradient operator $(\partial/\partial x, \partial/\partial y)$ and $\mathbf{n}_H$ is the outward normal to the solid in the plane of the horizontal cross-section.

In general, this free boundary problem for R_0 does not have a closed-form solution. We expect that at $z_v = 0$ the cross-section of the solid vanishes, and as z_v increases the cross-sectional area of the solid

increases. For small z_v we expect the cross-section will be axisymmetric. As z_v increases further, however, the cross-section of the solid will lose axial symmetry as it feels the presence of the cell boundary. While we are not able to find an explicit solution to describe the development of this asymmetry in the tail region, we can derive an explicit solution for the variation in the cross-sectional area of the solid. With this description of the cross-sectional area as a function of z_v we shall be able to match the inner and outer solutions by making the reasonable assumption that the cross-section is axisymmetric as $z_v \to 0$.

The description of the z_v variation in the cross-sectional area follows from conservation of solute. Equation (127) states that there is a volumetric source of solute throughout the liquid. Since there is no flux through the cell walls by equation (131), all the solute generated in the volume of the liquid must be balanced by a solute flux at the solid–liquid interface. This solute flux at the solid–liquid boundary thus determines the evolution of the shape $R_0(\theta, z_v)$ through equation (129).

To determine the explicit dependence of the cross-sectional area on z_v we let $\mathscr{A}(z_v)$ be the cross-sectional area, where

$$\mathscr{A}(z_v) = \int_0^{2\pi} \int_0^{R_0(\theta, z_v)} r \, dr \, d\theta = \int_0^{2\pi} (1/2) R_0^2 \, d\theta. \tag{132}$$

By Green's theorem in two dimensions,

$$\int_{\mathscr{L}} \nabla_H^2 C_l \, dA = -\int_{\mathscr{B}_S} (\mathbf{n}_H \cdot \nabla_H C_l) \, ds + \int_{\mathscr{B}_C} (\mathbf{n}_{cell} \cdot \nabla_H C_l) \, ds \tag{133}$$

where $\mathscr{L}$ is the liquid region, $\mathscr{B}_S$ is the surface of the solid, $\mathscr{B}_C$ is the boundary of the cell, and dA and ds denote differentials of cross-sectional area and arclength, respectively. The difference in the signs of the terms on the right-hand side is due to the fact that one of the normals ($\mathbf{n}_H$) points into the liquid region and the other ($\mathbf{n}_{cell}$) points out of the liquid region. We use equations (127), (129) and (131) and the fact that the cross-sectional area of the liquid is $\Lambda_x \Lambda_y - \mathscr{A}(z_v)$ to rewrite equation (133) as

$$\Lambda_x \Lambda_y - \mathscr{A}(z_v) = \int_{\mathscr{B}_S} \frac{\partial R_0}{\partial z_v} [1 + (1-k) z_v] \times \left[1 + \frac{1}{R_0^2} \left(\frac{\partial R_0}{\partial \theta} \right)^2 \right]^{-1/2} dS. \tag{134}$$

We rewrite the integral on the right-hand side using

$$dS = \left[1 + \frac{1}{R_0^2} \left(\frac{\partial R_0}{\partial \theta} \right)^2 \right]^{1/2} R_0 \, d\theta \tag{135}$$

and integrate the result using equation (132) to give

$$\Lambda_x \Lambda_y - \mathscr{A}(z_v) = [1 + (1-k) z_v] \frac{d\mathscr{A}}{dz_v}. \tag{136}$$

We solve this first-order, separable, ordinary differential equation to find

$$\mathscr{A}(z_v) = \Lambda_x \Lambda_y - \mathscr{A}_0 [1 + (1-k) z_v]^{-1/(1-k)} \tag{137}$$

where $\mathscr{A}_0$ is a constant of integration. We determine $\mathscr{A}_0 = \Lambda_x \Lambda_y$ by requiring the cross-sectional area to vanish as $z_v \to 0$.

Thus, the cross-sectional area of the solid in the tail region is given by

$$\mathscr{A}(z_v) = \Lambda_x \Lambda_y \{1 - [1 + (1-k) z_v]^{-1/(1-k)}\}. \tag{138}$$

This solution has the property that as $z_v \to \infty$, $\mathscr{A} \to \Lambda_x \Lambda_y$, indicating complete solidification of the liquid region. In our case, however, the domain is truncated at $z_v = (C_E/C_\infty - 1)/(1-k)$ by the formation of the eutectic phase.

4.8. *Matching the tail to inner and outer solutions*

To match the tail solution to the inner and outer solutions, we consider the behavior of these solutions in an intermediate region where $1 \ll z \ll 1/\epsilon$. We let $z_\dagger = \epsilon^\beta z$ be the z coordinate in the intermediate region where $0 < \beta < 1$. Consider now the tail solution in the intermediate region. The cross-sectional area of the tail is given in terms of $z_\dagger$ by

$$\mathscr{A}(\epsilon^{1-\beta} z_\dagger) \sim \epsilon^{1-\beta} \Lambda_x \Lambda_y z_\dagger. \tag{139}$$

If we assume that the cross-section $\mathscr{A}$ is axisymmetric as it vanishes, then we may deduce that the shape of the tail solution in the intermediate region is given by

$$R^2 \sim \epsilon^{1-\beta} \frac{\Lambda_x \Lambda_y}{\pi} z_\dagger. \tag{140}$$

We now compare this tail solution to the inner solution. From the inner solution 47, the scaling (34) and the matching condition (65), we determine that the dendrite shape in terms of the intermediate variable is

$$R^2 = \frac{\epsilon}{\pi \delta} \int_0^{z_\dagger/\epsilon^\beta - 2/\delta} q(\zeta') \, d\zeta'. \tag{141}$$

Matching the tail shape [relation (140)] and the inner shape [equation (141)] requires that the source strength $q(\zeta)$ must decay as

$$q(\infty) = \delta \Lambda_x \Lambda_y. \tag{142}$$

This behavior for $q(\zeta)$ is consistent with the integral equation for $q(\zeta)$ given by the inner/outer matching equation (66). As $\zeta \to \infty$, the dominant terms of equation (66) are

$$\delta \zeta \sim \int_0^\infty q(\zeta') G_{array}(\zeta; \zeta') \, d\zeta'. \tag{143}$$

After a lengthy and detailed asymptotic analysis of

the integral on the right-hand side, it is possible to show that

$$\int_0^\infty q(\zeta')G_{\text{array}}(\zeta;\zeta')\,d\zeta' \sim \frac{q(\infty)}{\Lambda_x\Lambda_y}\zeta \quad \text{as } \zeta\to\infty. \tag{144}$$

Thus, relation (143) gives, as a consequence of inner/outer matching, the same result as equation (142) for $q(\infty)$.

Thus, the solution of the inner/outer equation (66) requires a particular behavior for the source strength $q(\infty)$. This behavior for the source strength is precisely that required to match the tail solution, and the tail, inner and outer solutions match automatically. We have now completed the asymptotic matching of inner, outer, tip and tail solutions.

4.9. *Composite solution*

From our matched, locally valid solutions in the tip, inner, outer and tail regions (see Fig. 4) we can construct a uniformly valid leading-order solution for the shape of each dendrite and the concentration field in its surrounding periodic unit cell.

We have determined the shape of the needle crystal in cylindrical coordinates (r, ζ, θ) where $\zeta = z - z_{\text{tip}}$ measures the distance behind the dendrite tip. The composite solution for the dendrite shape is given by $r = R_{\text{comp}}$ with

$$R_{\text{comp}} = R_{\text{in}} + R_{\text{tip}} - R_{\text{tip/in}} + R_{\text{tail}} - R_{\text{tail/in}}. \tag{145}$$

In the above, the notation $R_{\text{tip/in}}$ refers to the common part of the tip and inner solutions, which we matched in the tip/inner overlap region. Using the results of our analysis, the composite solution for the shape can be written as

$$R_{\text{comp}}(\zeta,\theta) = \epsilon^{1/2}\bar{R} + R_{\text{tail}}(\zeta,\theta) - \sqrt{\epsilon\Lambda_x\Lambda_y\zeta/\pi} \tag{146}$$

where R_{tail} is the nonaxisymmetric tail shape that has a cross-sectional area given by

$$\mathscr{A}(\zeta) = \Lambda_x\Lambda_y\{1 - [1 + (1-k)\epsilon\zeta]^{-1/(1-k)} \tag{147}$$

and $\bar{R}(\zeta)$ is the shape of the dendrite in the inner region. The inner shape $\bar{R}(\zeta)$ is given by

$$\bar{R}(\zeta) = \sqrt{\frac{1}{\pi\delta}\int_0^\zeta q(\zeta')\,d\zeta'} \tag{148}$$

where $q(\zeta)$ is a solute line source that extends from $0 < \zeta < \infty$. The line source $q(\zeta)$ satisfies the nonlinear integral equation

$$\mathscr{I} + \delta\zeta = \frac{q(\zeta)}{4\pi\delta} - \frac{q(\zeta)}{4\pi}\left[\ln\left(\frac{\bar{R}^2}{4\zeta}\right) + \gamma_{\text{E}}\right] + \int_0^\infty [q(\zeta') - q(\zeta)]G_{\text{near}}(\zeta;\zeta')\,d\zeta' + \int_0^\infty q(\zeta')G_{\text{array}}(\zeta;\zeta')\,d\zeta'. \tag{149}$$

In the above equation, $\mathscr{I}$ is the unknown tip position, γ_{E} is Euler's constant, and G_{near} and G_{array} are given by equations (60) and (62). The solution to the integral equation $q(\zeta)$ is linked to the scaled tip radius P by

$$P = \frac{q(0)}{2\pi\delta} \tag{150}$$

and $q(\zeta)$ is also linked to the tail solution by

$$q(\infty) = \delta\Lambda_x\Lambda_y. \tag{151}$$

Therefore, to determine $\bar{R}$ appearing in the composite solution for the shape, we need to solve the integral equation (149) subject to the constraints (150) and (151).

The composite solution for the concentration field in the unit cell surrounding each dendrite is given by

$$C_{\text{comp}} = C_{\text{in}} + C_{\text{tip}} - C_{\text{tip/in}} + C_{\text{out}} - C_{\text{out/in}} + C_{\text{tail}} - C_{\text{tail/in}}. \tag{152}$$

Using the results of our analysis, we can write C_{comp} as

$$C_{\text{comp}}(x,y,\zeta) = -(\epsilon P/2)\ln\left\{\frac{2\zeta}{r^2}\left[\sqrt{r^2 + (\zeta - (\epsilon P/2))^2} - (\zeta - (\epsilon P/2))\right]\right\} + \frac{\epsilon}{\delta}\sum_{i=-\infty}^{\infty}\sum_{j=-\infty}^{\infty} \times \int_0^\infty q(\zeta')G_{ij}(x,y,\zeta;\zeta')\,d\zeta' \tag{153}$$

where G_{ij} is the Green's function given by equation (53), and $q(\zeta)$ is the solute line source strength determined from equations (149)–(151).

Finally, in our model these solutions are truncated at $z = (C_{\text{E}}/C_\infty - 1)/(\epsilon(1-k))$ where any remaining liquid changes to solid eutectic.

5. DISCUSSION

Our analysis of the free boundary problem for a periodic array of needle crystals included a determination of locally valid solutions in each of the four asymptotic regions. By matching the solutions in each of the overlap regions we were able to determine an equation describing the shape of the dendrite. This equation is independent of the surface energy (as we specifically set the surface energy term to zero to obtain the tip solution). We shall suggest in this section that our equation for the shape contains within it a specific mechanism for selection of the tip radius, and therefore surface energy considerations are not required to determine the tip radius of the dendrite. Thus, for a given set of experimental conditions, our integral equation has a family of

solutions parameterized only by the spacing of the array.

First, we show that for infinite dendrite spacing and zero temperature gradient we recover the isolated, isothermal, Ivantsov dendrite with solute undercooling. For infinite array spacing we set $\Lambda_x = \Lambda_y = \infty$ causing G_{array} in equation (149) to vanish. Further, for infinite array spacing there is no longer a tail region, so equation (151) no longer applies and the full composite solution is identically given by R_{in}. To separate the effects of the temperature gradient and the tip undercooling we note that the left-hand side of the integral equation (149) can be written as

$$\mathscr{Z} + \delta\zeta = (\delta/\epsilon)\Theta + G\zeta(D\delta)/(\epsilon k\, \Delta T_0 V) \qquad (154)$$

where $\Theta = (T_0 - T_{\text{tip}})/(k\, \Delta T_0)$ is the nondimensional solute undercooling of the tip and the term proportional to $G\zeta$ represents the temperature gradient. We eliminate the temperature gradient by setting $G\zeta = 0$ and substitute equation (154) into equation (149) to obtain an equation for the isolated, isothermal solute dendrite:

$$\frac{\delta}{\epsilon}\Theta = \frac{q(\zeta)}{4\pi\,\delta} - \frac{q(\zeta)}{4\pi}\left[\ln\left(\frac{\bar{R}^2}{4\zeta}\right) + \gamma_{\text{E}}\right] + \int_0^\infty [q(\zeta') - q(\zeta)]G_{\text{near}}(\zeta;\zeta')\,\mathrm{d}\zeta' \qquad (155)$$

with $q(0) = 2\pi\delta P$ and $q(\infty)$ unprescribed. This integral equation and constraint is satisfied by $q(\zeta) = 2\pi\delta P$ (constant), where

$$\Theta = (\epsilon P/2)[-\ln(\epsilon P/2) - \gamma_{\text{E}}] \qquad (156)$$

and $R = \sqrt{2\epsilon P\zeta}$. This solution is an Ivantsov paraboloid. The relation (156) corresponds to the first two terms of the familiar Ivantsov relation

$$\Theta = (\epsilon P/2)E_1(\epsilon P/2)\exp(\epsilon P/2) \qquad (157)$$

when expanded for $\epsilon P \ll 1$. Thus, for infinite spacing and zero temperature gradient we recover the small Peclet number Ivantsov solution. For this solution, there is no tip selection. The undercooling determines ρ/l_{D} but a family of solutions exist with ρ/l_{D} = constant.

In a subsequent paper we shall solve the integral equation (149) numerically to determine the dendrite shape as a function of the process parameters [3]. We shall show that for a given set of experimental conditions and dendrite spacings (δ, Λ_x and Λ_y prescribed) the integral equation (149) has a unique solution for the tip position $\mathscr{Z}$ and source strength $q(\zeta)$. The decay condition (151) is satisfied by the solutions automatically, and the value of $q(\zeta)$ at $\zeta = 0$ determines the tip radius of the dendrite. Thus, a consequence of our model is that selection of the tip radius is due to the presence of neighboring dendrites and does not rely on the effect of surface energy.

The idea of the tip radius being directly related to the dendrite spacing has been suggested previously [2, 17]. In the earlier papers, simple models for the dendrite shape were proposed, which led to the spacing being a function of the tip radius. The emphasis at the time was to use a criterion to select a unique tip radius that would give a unique spacing for the array. Our approach is different in that we have shown explicitly that by considering the nonlinear interactions between dendrites and solving for the nontrivial details of the shape we can obtain a unique solution. Hence, our view is that the dendrite spacings determine the tip characteristics and not the other way around.

In the spirit of these earlier papers we present a simplified explanation as to why the spacing of the array might select a tip radius. Consider the directional solidification process with a weak temperature gradient ($l_{\text{D}} \ll l_{\text{T}}$). Instead of an array of dendrites, think of a single dendrite growing in the center of a cylindrical tube of dimensional radius R_λ. Here, R_λ mimics the dendrite spacing λ, with the no-flux boundary conditions on the walls of the tube corresponding to the symmetry conditions at the boundary of a periodic unit cell for the array. At the tip of the dendrite, provided the walls are far enough away, we can neglect the walls and describe the dendrite tip in dimensional variables as an Ivantsov paraboloid:

$$R_{\text{tip}}^2 = 2\rho(z - z_{\text{tip}}) \qquad (158)$$

with

$$\frac{T_0 - T_{\text{tip}}}{k\, \Delta T_0} = (\rho/2l_{\text{D}})E_1(\rho/2l_{\text{D}})\exp(\rho/2l_{\text{D}}). \qquad (159)$$

Now consider the region far behind the tip, $(z - z_{\text{tip}}) = O(l_{\text{T}})$. Here, the shape is controlled by the weak temperature gradient and the nearness of the tube walls to the dendrite surface. There is a slow variation of all quantities in the z direction and uniform concentration in the radial direction. The Scheil-type solution for the tail region can be determined from conservation of mass in the tail region to be

$$R_{\text{tail}}^2 = R_\lambda^2\{1 - [1 + (1-k)(z - z_{\text{tip}})/l_{\text{T}}]^{-1/(1-k)}\}. \qquad (160)$$

The basic idea underlying our analysis is that there is a self-consistent solution for the shape that satisfies all the governing equations and describes the transition from the Ivantsov tip to the Scheil-type tail. In our full model this transition is accomplished by the inner solution and requires the solution of the integral equation (149). For this simplified explanation the analogy requires the Ivantsov tip [equation (158)] and the Scheil-like tail [equation (160)] to match in between the tip and tail regions, when

$\rho \ll z - z_{tip} \ll l_T$. In this case the tail solution behaves like

$$R_{tail}^2 \sim R_\lambda^2 \frac{z - z_{tip}}{l_T} \tag{161}$$

so matching to the Ivantsov tip requires

$$\frac{R_\lambda^2}{l_T} = 2\rho. \tag{162}$$

For the directional solidification geometry we know l_T, so equation (162) gives a unique ρ for each "spacing" R_λ. References [2] and [17] have similar relationships between the tip radius and the spacing. While the above illustrates the idea of what underlies the tip selection in our theory, relationship (162) is not correct because the two solution pieces in our simple model, even when matched, do not solve the free boundary problem. To determine the correct relationship between the tip radius and the dendrite spacing, one must actually solve for the transitional inner shape $\bar{R}$ which connects the tip and tail solutions from equations (148)–(151). This solution for $\bar{R}$ necessarily involves the interaction of the shape with the neighboring dendrites in the array, and is consequently somewhat complicated, but the idea is the same.

In a sequel to this paper [3] we compare the predictions of our theory to the experimental results on the growth of dendrite arrays during directional solidification of SCN-acetone [7]. We will show that when our expansion parameter $\epsilon = l_D/l_T$ is small, our theory agrees well with experimental data. It is on the basis of this correspondence with experiment that we claim our smooth solutions are relevant when describing dendrite morphologies. The point of view of our theory is that the growth of dendrite arrays at moderate velocities† is not controlled by surface energy considerations and can be described well by ignoring the presence of sidebranches in favor of an "averaged" needle crystal. The dendrite spacings would be determined interactively by the growth process [18], but the tip characteristic would follow from the dendrite spacings and not criteria based on surface energy considerations.

We appreciate that in suggesting that the tip radius of a dendrite is not selected by surface energy we are departing from the generally accepted view of dendritic growth [5, 18]. However, since our results compare favorably with experimental data, we put the model forward as an alternative description of dendritic arrays in directional solidification. An interesting issue yet to be addressed is the effect of including surface energy in our model to determine if spacing-selected and surface-energy-selected states can be reconciled. A further issue is the confirmation of the appropriateness of needle crystal solutions to describing the characteristics of dendritic growth. While our results suggest that the tip characteristics of dendrite arrays can be described by ignoring sidebranches and neglecting surface energy, we must leave open the possibility that these features are important to describing dendrite tip characteristics in some parameter regimes. The presence of sidebranches may effectively remove any necessity to match to a tail solution, in which case the dendrite would be free to modify its tip radius in accord with a local surface-energy-based solvability condition. We do not claim that this view is necessarily incorrect, but in the absence of evidence to the contrary we put our model forward as a viable theory that corresponds to the experimental observations. As such, our model is an interesting alternative to the traditional view, and should be considered further to understand its relevance and implications for the growth of dendrite arrays.

†At high velocities, when $l_C \sim \rho$, surface energy will not be negligible.

Acknowledgements—This research is funded by a grant from the EPSRC. We are grateful to D. M. Anderson, S. H. Davis, E. J. Hinch, J. R. Lister, and M. G. Worster for many valuable discussions over the course of this work.

REFERENCES

1. Ivantsov, G. P., *Dokl. Akad. Nauk. SSSR*, 1947, **58,** 567.
2. Hunt, J. D., in: *Solidification and Casting of Metals*. The Metals Society, London, 1979, p. 3.
3. Spencer, B. J. and Huppert, H. E., *Acta metall. mater.*, preprint, 1996.
4. Langer, J. S., *Rev. Mod. Phys.*, 1980, **52,** 1.
5. Trivedi, R. and Kurz, W., *Acta metall. mater.*, 1994, **42,** 15.
6. Trivedi, R., *J. Crystal Growth*, 1980, **49,** 219.
7. Somboonsuk, K., Mason, J. T. and Trivedi, R., *Metall. Trans. A*, 1984, **15A,** 967.
8. Warren, J. A. and Langer, J. S., *Phys. Rev. A*, 1990, **42,** 3518.
9. Hinch, E. J., *Perturbation Methods*. Cambridge University Press, Cambridge, 1992.
10. Mullins, W. W. and Sekerka, R. F., *J. Appl. Phys.*, 1964, **35,** 444.
11. Xu, J. J., in: *Structure and Dynamics of Partially Solidified Systems*, ed. D. E. Loper. Martinus Nijhoff, Dordrecht, 1987, p. 97.
12. Spencer, B. J. and Huppert, H. E., *J. Crystal Growth*, 1995, **148,** 305.
13. Langer, J. S. and Müller-Krumbhaar, H., *Acta metall.*, 1978, **26,** 1681.
14. Xu, J. J., *Phys. Rev. A*, 1991 **43,** 930.
15. Ben Amar, M. and Brener, E., *Phys. Rev. Lett.*, 1993, **71,** 589.
16. Brener, E., *Phys. Rev. Lett.*, 1993, **71,** 3653.
17. Kurz, W. and Fisher, D. J., *Acta metall.*, 1981, **29,** 11.
18. Han, S. H. and Trivedi, R., *Acta metall. mater.*, 1994, **42,** 25.